

Article

A Feature of Mechanics-Driven Statistical Moments of Wavelet Transform-Processed Dynamic Responses for Damage Detection in Beam-Type Structures

Jinwen Huang ^{1,2}, Tongfa Deng ^{1,2,*}, Maosen Cao ^{1,3}, Xiangdong Qian ³  and Mahmoud Bayat ^{4,5}

¹ Jiangxi Province Key Laboratory of Environmental Geotechnical Engineering and Hazards Control, Jiangxi University of Science and Technology, Ganzhou 341000, China

² School of Civil and Surveying & Mapping Engineering, Jiangxi University of Science and Technology, Ganzhou 341000, China

³ Department of Engineering Mechanics, Hohai University, Nanjing 210098, China

⁴ Department of Civil and Environmental Engineering, University of South Carolina, Columbia, SC 29208, USA

⁵ Ingram School of Engineering, Texas State University, San Marcos, TX 78666, USA

* Correspondence: tfdeng@jxust.edu.cn; Tel.: +86-139-7078-3208



Citation: Huang, J.; Deng, T.; Cao, M.; Qian, X.; Bayat, M. A Feature of Mechanics-Driven Statistical Moments of Wavelet Transform-Processed Dynamic Responses for Damage Detection in Beam-Type Structures. *Appl. Sci.* **2022**, *12*, 11561. <https://doi.org/10.3390/app122211561>

Academic Editor: Abílio Manuel Pinho de Jesus

Received: 24 October 2022

Accepted: 8 November 2022

Published: 14 November 2022

Publisher's Note: MDPI stays neutral with regard to jurisdictional claims in published maps and institutional affiliations.



Copyright: © 2022 by the authors. Licensee MDPI, Basel, Switzerland. This article is an open access article distributed under the terms and conditions of the Creative Commons Attribution (CC BY) license (<https://creativecommons.org/licenses/by/4.0/>).

Abstract: Multiple damage detection using structural responses only is a problem unresolved that is in the field of structural health monitoring. To address this problem, a novel feature of mechanics-driven statistical moments of wavelet transform-processed dynamic responses is proposed for multi-damage identification in beam-type structures. This feature is referred to as a continuous wavelet transform (CWT)-second-order strain statistical moment (SSSM), with CWT-SSSM in the abbreviation. The mechanical connotation of CWT-SSSM lies in that the SSSM of each order principal vibration contains strain mode shapes, inducing greater sensitivity to local damage. With this method, the CWT is used to extract and amplify the singularities caused by damage in each order SSSM curve, following which the data fusion technology and three-sigma rule in statistics are adopted to construct the damage index. The presence of damage is characterized by the abrupt change in the damage index. The soundness and characteristics of the CWT-SSSM feature are verified by identifying multiple damages in a cantilever beam bearing two breathing cracks. The results show that the proposed feature can accurately designate multiple cracks free of baseline information on the intact counterpart; moreover, it has robustness against noise and applicability under excitations of approximately uniform spectra.

Keywords: damage detection; CWT; SSSM; dynamic response; strain mode shapes; baseline-free damage feature; noise robustness; beam-type structure

1. Introduction

In the areas of mechanical, civil, and transportation engineering, structural components are inevitably damaged in their long-term service process due to the coupled influence of multiple factors, typically material deterioration, environmental corrosion, temperature stress, and external load. The occurrence of damage may decrease the service performance of the structure and even lead to catastrophic accidents. Hence, the identification of early damage is critical to maintaining the integrity and safety of the structure.

Compared with static damage identification, dynamic damage identification [1–3] has developed rapidly and attracted more and more researchers' attention. The main reasons are as follows: (i) This is a global damage detection pattern that does not require advanced knowledge of the local damage area. (ii) The dynamic response collected under environmental excitation can be used for damage identification analysis; furthermore, the normal use of the structure will not be affected during the experiment. (iii) With the rapid development of sensing technology, remote, and intelligent structural health monitoring can be realized.

Among the initial research on dynamic-based damage identification, the modal-based dynamic damage identification research is the most in-depth and representative, while a series of related joint methods have been developed [4]. Modal-based damage identification methods mainly identify damage by comparing changes in structural modal parameters (e.g., natural frequency [5], mode shapes [6], damping ratios [7]) or modal derivative quantities (e.g., curvature mode shapes [8], strain mode shapes [9], flexibility matrix [10], etc.) before and after the damage, which can mostly reveal the spatial information of structural damage. However, the following problems still exist in practical applications: (i) the selection of the order of the modal parameters significantly affects the accuracy and sensitivity of damage identification because the low-order modal parameters are insensitive to slight damage, and the high-order modal parameters are equally sensitive to noise, although they are excellent in discriminating slight damage; (ii) Not only can structural damage lead to changes in modal parameters, but also environmental factors (noise, temperature, humidity) may cause significant changes in modal parameters. (iii) Modal-based identification methods usually require complex modal processing of the measured dynamic response, and part of the effective information is inevitably lost in the process; in addition, for some large civil engineering structures, the higher-order modal parameters are difficult to measure accurately (especially the higher-order mode shapes).

Dynamic damage identification methods also include damage identifications that are based on signal processing [11–13] and damage identification based on statistical characteristics of the dynamic response. The latter utilizes statistical theory for damage detection directly in the time domain, and compared with other dynamic-based damage identification methods, this method is operationally simple and does not involve a complex modal processing procedure, which does not result in the loss of valid information. Moreover, this method combines a statistical theory in the field of mathematics, so it is highly resistant to the interference of measurement noise. A typical study using statistical characteristics of the dynamic response to identify the structural damage is as follows. Zhang et al. [14] first proposed a damage detection method based on statistical moments of dynamic response under Gaussian excitation. They combined the fourth-order statistical moment theory in the field of mathematical statistics to define a damage identification index that is sensitive to damage and insensitive to measurement noise. In subsequent studies, Zhang et al. [15,16] extended the method based on response statistical moments. Numerical simulations and shake table experiments on three-story shear-type buildings showed that their method was effective in assessing structural damage and identifying the damage severity even under non-stationary non-Gaussian excitation conditions. Based on the previous studies, Wang et al. [17,18] applied the statistical moment-based method to the damage identification study of beam-type structures. They improved the existing statistical moment theory and proposed a damage index based on fourth-order statistical moments of the strain response. The results of numerical simulations and simply supported beam experiments [19] proved the effectiveness and practicality of their method. Yang et al. [20] pointed out that the identification method based on statistical characteristics of the dynamic response can simplify the calculation. They used the cross-correlation function amplitude vector (CorV) of the measured dynamic response to evaluate the structural damage. The reliability of the method was demonstrated by experiments on the fastener loss of an aircraft panel model. The above studies show that the method based on the statistical characteristics of the dynamic response possesses great potential in revealing damage and is a reliable method for dynamic damage identification.

Most of the dynamic-based damage identification methods tend to locate the damage by comparing the baseline data from intact structures. In actual engineering structures, some structures that have been in service for a long time, such as complete baseline data, are difficult or even impossible to obtain. As a result, more and more scholars have developed baseline-free damage identification. Baseline-free dynamic damage identification methods are mainly divided into weak baseline-free methods and strong baseline-free methods. The weak baseline-free method mainly adopts the curve (surface) fitting technique to obtain the

baseline data (mode shapes and their derivatives, static deflection, etc.), and it is possible to compare the baseline data to locate the damage. Yoon et al. [21] carried out the baseline-free structural damage identification in composite plates using the two-dimensional gapped smoothing method. Wang et al. [22] used multi-segment function-fitting calculations to establish the deflection influence line (DIL) of a bridge without damage, and the damage location was detected by comparing the DIL before and after the damage. The strong baseline-free method, on the other hand, directly uses technical means such as wavelet transform, fractal dimension, and second-order central difference to process the damage data and characterize the occurrence of damage according to the abrupt peaks [23–25].

The above baseline-free methods achieved satisfactory results; however, there was a relatively complex data processing procedure when applying these methods. For example, when extracting mode shapes, a complex modal processing procedure must be undergone, which undoubtedly increases the computational cost. Moreover, known excitation information is usually required to construct the frequency response function of the structure. In addition, some valid information is lost when converting the time domain response to the frequency domain. In order to improve the computational efficiency and accuracy of damage identification, this paper proposes an identification method of structural multiple damages based on the CWT-SSSM feature by combining the statistical characteristics of the dynamic response and WT. The proposed method first selects the strain response, which is more sensitive to local damage for analysis, then utilizes CWT to highlight the damage singularity information in each order SSSM curve, and finally combines data fusion techniques and the three-sigma rule to construct the damage index of this paper. The proposed method is computationally simple, without the need for known excitation and baseline information, it enables the rapid localization of structural damage using only the output response.

The rest of the paper is organized as follows: Section 2 introduces the basic theory of continuous wavelet transform (CWT), empirical wavelet transforms (EWT), and the dynamic response statistical moment (DRSM). Section 3 defines the CWT-SSSM feature-based damage identification index and gives the damage identification flowchart. Section 4 establishes a damaged cantilever beam model containing two breathing cracks and applies the proposed method to identify the damage. Section 5 discusses the noise robustness of the proposed method as well as the excitation applicability. The conclusions are presented in Section 6.

2. Fundamentals

This section introduces the basic theory of continuous wavelet transform, empirical wavelet transforms, and the dynamic response statistical moment.

2.1. Continuous Wavelet Transform (CWT)

The CWT of the signal $f(t) \in L^2(\mathbb{R})$ can be expressed as the following formula [26]:

$$Wf(b,s) = f * \frac{1}{\sqrt{s}} \bar{\varphi}(b/s) = f * \bar{\varphi}_s(b) = \int_{-\infty}^{+\infty} f(x) \bar{\varphi}_{b,s} dx \quad (1)$$

where $Wf(b,s)$ is the CWT coefficient of $f(t)$, $\varphi(x)$ is the wavelet function, b and s are the translation and scale parameters, respectively, $\bar{\cdot}$ denotes the conjugate operation, and $*$ denotes the convolution operation. In the field of signal processing, CWT is the most commonly used tool for time-frequency analysis, which can effectively portray the local characteristics of signals.

2.2. Empirical Wavelet Transform (EWT)

Gilles proposed the EWT based on EMD (empirical mode decomposition) using the wavelet transform as the theoretical framework [27]. The detail coefficients $W_f^e(n, t)$ and the approximation coefficients $W_f^e(0, t)$ of EWT can be expressed as follows:

$$W_f^e(n, t) = \langle f(t), \psi_n(t) \rangle = \int f(\tau) \overline{\psi_n(\tau - t)} d\tau \quad (2)$$

$$W_f^e(0, t) = \langle f(t), \varphi_1(t) \rangle = \int f(\tau) \overline{\varphi_1(\tau - t)} d\tau \quad (3)$$

where $\psi_n(t)$ and $\varphi_1(t)$ are the empirical wavelet function and the scale function, respectively, and $f(t)$ can be reconstructed by the following formula:

$$f(t) = W_f^e(0, t) * \varphi_1(t) + \sum_{n=1}^N W_f^e(n, t) * \varphi_n(t) \quad (4)$$

In the field of structural modal parameter identification, the intrinsic mode function (IMF) component can be separated from the response signal by EWT, and the modal parameters of the structure can be obtained by analyzing the IMF [28].

2.3. Dynamic Response Statistical Moment (DRSM)

If an excitation force subject to a stationary Gaussian random process distribution is applied to a linear structural system, then the output response x of the system will be subject to a stationary Gaussian random process distribution [15]. To this end, the n th-order statistical moment of the dynamic response x can be expressed as:

$$DRSM_n = \frac{1}{\sigma\sqrt{2\pi}} \int_{-\infty}^{+\infty} (x - \mu)^n e^{-\frac{(x-\mu)^2}{2\sigma^2}} dx \quad (5)$$

where μ and σ are the mean and standard deviation of the response x , respectively. From Formula (5), it is easy to verify that when n is odd, $DRSM_n = 0$ and when n is even, $DRSM_n = 1 \cdot 3 \cdot 5 \cdot \dots \cdot (n-1)\sigma^n$.

The above formula works under the condition that the excitation force on the structure obeys a stationary Gaussian random process distribution. Under general excitation, the expression of $DRSM_n$ in the time domain can be expressed as the following formula:

$$DRSM_n = \frac{1}{N} \sum_{r=1}^N (x_r - \mu)^n \quad (6)$$

where N is the number of the sampling points.

3. CWT-SSSM Feature-Based Damage Index

This part analyzes the relationship between SSSM and the strain mode from a mechanical perspective, then establishes the damage identification index $SSSM_{DI}$, and finally introduces the identification steps based on the CWT-SSSM feature method in the form of flowcharts.

3.1. Second-Order Strain Statistical Moments (SSSM)

For a multi-degree-of-freedom linear structural system, under the action of Gaussian white noise $F(t)$ with a mean value of 0 and power spectral density S_0 , its motion differential equation can be expressed as:

$$M\ddot{x} + C\dot{x} + Kx = F(t) \quad (7)$$

where \ddot{x} , \dot{x} , and x are the acceleration, velocity, and displacement responses of the structure under white noise excitation, respectively. M , C , and, K are the mass, damping, and stiffness matrices of the structure, respectively.

Adopting the assumption of Rayleigh damping, the displacement response $x(t)$ can be solved by the modal decomposition method:

$$x(t) = \sum_{i=1}^n z_i(t) \varphi_i \quad (8)$$

where $z_i(t)$ is the i th-order modal coordinate and φ_i is the i th-order mode shape. If the excitation force acts only on the r th degree of freedom, then the displacement frequency response function $H_{sr}(\omega)$ on the s th degree of freedom can be expressed as:

$$H_{sr}(\omega) = \sum_{i=1}^n \frac{\varphi_{si}\varphi_{ri}}{\bar{m}_i(\omega_i^2 - \omega^2 + 2j\omega\omega_i\zeta_i)} \quad (9)$$

where \bar{m}_i , \bar{c}_i , and \bar{k}_i are the i th-order modal mass, modal damping, and modal stiffness, respectively. ω_i , and ζ_i are the i th-order natural frequency and damping ratio, respectively.

It is worth mentioning that the strain response is more sensitive to local damage than the displacement response [29–32] because the strain mode shape is a second-order differentiation of the displacement mode shape, while the differentiation operation further amplifies the abrupt changes in the curve caused by damage. Consequently, the strain response data are selected for the damage identification study. The strain response $\varepsilon(t)$ can also be solved by the modal decomposition method.

$$\varepsilon(t) = \sum_{i=1}^n z'_i(t) \psi_i \quad (10)$$

where $z'_i(t)$ is the i th-order modal coordinate corresponding to the strain, which represents the contribution of the i th-order strain mode ψ_i to the strain response, as well as $z_i(t) = z'_i(t)$. The strain frequency response function $H_{sr}^\varepsilon(\omega)$ can be expressed as the following formula:

$$H_{sr}^\varepsilon(\omega) = \sum_{i=1}^n \frac{\psi_{si}\varphi_{ri}}{\bar{m}_i(\omega_i^2 - \omega^2 + 2j\omega\omega_i\zeta_i)} \quad (11)$$

According to the theory related to random vibration, the second-order strain statistical moment $SSSM_s$ (variance) of the s th degree of freedom can be written as the following formula:

$$SSSM_s = \sigma^2 = \int_{-\infty}^{+\infty} H_{sr}^\varepsilon(\omega) \overline{H_{sr}^\varepsilon(\omega)} S_0 d\omega \quad (12)$$

In this paper, we focus on the second-order statistical moment because the higher-order statistical moment is unstable [18]. In addition, it is noted that the $H_{sr}^\varepsilon(\omega)$ in Formula (11) takes into account the contribution of all the strain mode shapes. Under the premise that only the contribution of the i th-order strain mode shape is considered, Formulas (11) and (12) can be rewritten as:

$$H_{sr}^{ei}(\omega) = \frac{\psi_{si}\varphi_{ri}}{\bar{m}_i(\omega_i^2 - \omega^2 + 2j\omega\omega_i\zeta_i)} \quad (13)$$

$$SSSM_s^i = \int_{-\infty}^{+\infty} H_{sr}^{ei}(\omega) \overline{H_{sr}^{ei}(\omega)} S_0 d\omega = \int_{-\infty}^{+\infty} |H_{sr}^{ei}(\omega)|^2 S_0 d\omega = \frac{\pi S_0 \psi_{si}^2 \varphi_{ri}^2}{2\zeta_i \sqrt{\bar{m}_i \bar{k}_i}^3} \quad (14)$$

where $SSSM_s^i$ is the SSSM considering only the i th-order principal vibration in the s th degree of freedom; furthermore, $SSSM_s^i$ is only related to the i th-order strain modal parameters (ψ_{si} , \bar{m}_i , ζ_i , and \bar{k}_i) and the white noise excitation (S_0 and φ_{ri}). If the linear structural system

contains m degrees of freedom, then the second-order strain statistical moment $SSSM^i$ for these degrees of freedom considering only the i th-order strain modal contribution can be expressed as:

$$SSSM^i = [SSSM_1^i, SSSM_2^i, SSSM_3^i, \dots, SSSM_m^i] = [R_i \psi_{1i}^2, R_i \psi_{2i}^2, R_i \psi_{3i}^2, \dots, R_i \psi_{mi}^2] \quad (15)$$

$$R_i = \frac{\pi S_0 \varphi_{ri}^2}{2\zeta_i \sqrt{m_i k_i^3}} \quad (16)$$

Formula (15) shows that the second-order strain statistical moment $SSSM^i$ considering only the i th-order principal vibration contains the strain mode shape, which is more sensitive to local damage.

It is worth mentioning that in practical applications, $SSSM^i$ can be calculated in the time domain with a very simple calculation procedure. Taking $SSSM_m^i$ as an example, firstly, EWT is used to separate the strain response IMF_m^i considering only the i th-order principal vibration, and then $SSSM_m^i$ is directly calculated by substituting IMF_m^i into Formula (6). It is expressed in the formula as:

$$SSSM_m^i = \sigma_{mi}^2 = \frac{1}{N} \sum_{r=1}^N (IMF_m^i(r) - \mu)^2 \quad (17)$$

where N denotes the number of sampling points of IMF_m^i , and μ is the mean value of IMF_m^i .

3.2. Damage Index (DI)

The occurrence of damage inevitably leads to a reduction in the local stiffness of the structure, which in turn leads to singularities (differential discontinuities) in the mode shapes at the location of the damage. CWT is known as a signal microscope that can detect singularities in the mode shapes. It has been demonstrated above in the frequency domain that $SSSM^i$ contains the i th-order strain modal, and, in particular, it contains strain mode shapes that are sensitive to local damage. Therefore, it is possible to locate the damage location based on the abrupt change in the spatial location of the CWT coefficients of $SSSM^i$.

In this paper, CWT- $SSSM^i$ is defined as $CS^i(b, s)$. A strain response can be separated into multiple-order strain components of IMF^e using EWT, thus the corresponding IMF^e also has multiple orders. Different orders of IMF^e have different sensitivities to the same damage, and for multi-damage identification, it may be difficult to accurately identify all the damage locations by using only the one order $CS(b, s)$. For this purpose, the data fusion technique of averaging is used to integrate all orders of $CS(b, s)$, and the overall CWT- $SSSM$ is defined as:

$$\overline{CS}(b, s) = \frac{1}{n} \sum_{i=1}^n \text{normalize}(CS^i(b, s)) \quad (18)$$

where $\text{normalize}(CS^i(b, s))$ represents the maximum normalization of $CS^i(b, s)$, which can be expressed as: $\text{normalize}(CS^i(b, s)) = CS^i(b, s) / \max(|CS^i(b, s)|)$, and the superscript i represents the order. $\overline{CS}(b, s)$ fuses damage information of all the orders but $\overline{CS}(b, s)$ characterizes the occurrence of damage with abrupt peaks in the 3D plot, while the smaller peaks due to noise could confuse the user's judgment. For this reason, this paper combines statistical theory to construct the damage identification index $SSSM_{DI}$:

$$SSSM_{DI} = \begin{cases} T(b), & \text{if } T(b) \geq SSSM_{DI}^{TH} \\ 0, & \text{if } T(b) \leq SSSM_{DI}^{TH} \end{cases} \quad (19)$$

where,

$$T(b) = \sum_{s=1}^{s_{\max}} \overline{CS}(b, s) \quad (20)$$

$$SSSM_{DI}^{TH} = \mu + 3\sigma \quad (21)$$

In the above formula, s_{\max} represents the maximum scale. $SSSM_{DI}^{TH}$ is the damage threshold defined and based on the three-sigma rule in statistics, μ and σ are the mean and standard deviation of $T(b)$, respectively. The probability of a normal distribution with values distributed at $(\mu - 3\sigma, \mu + 3\sigma)$ is 99.73%. For damage detection, if the value of the $SSSM_{DI}$ index of a measurement point exceeds the range of $(\mu - 3\sigma, \mu + 3\sigma)$, the structural health monitoring system has a 99.7% certainty that the damage occurs at this measurement point. Hence, for damage assessment, the location of the damage can be located based on the peak of $SSSM_{DI}$.

3.3. Damage Identification Process

The index $SSSM_{DI}$ constructed in the above way possesses the following advantages: ① The calculation process of $SSSM^i$ is extremely simple without a complex modal processing procedure; furthermore, it does not require known excitation data and baseline information before the damage. ② $SSSM^i$ contains strain mode shapes, which are more sensitive to damage than displacement modes, and the strain is less expensive to monitor than displacement and acceleration. ③ $SSSM_{DI}$ fuses the damage information of multi-order $CS(b, s)$ and introduces the damage threshold $SSSM_{DI}^{TH}$ based on the three-sigma rule, which makes $SSSM_{DI}$ have a higher identification sensitivity and localization accuracy for multiple damages and a stronger immunity to noise interference. Figure 1 shows the flow chart of the damage identification based on the CWT-SSSM feature method.

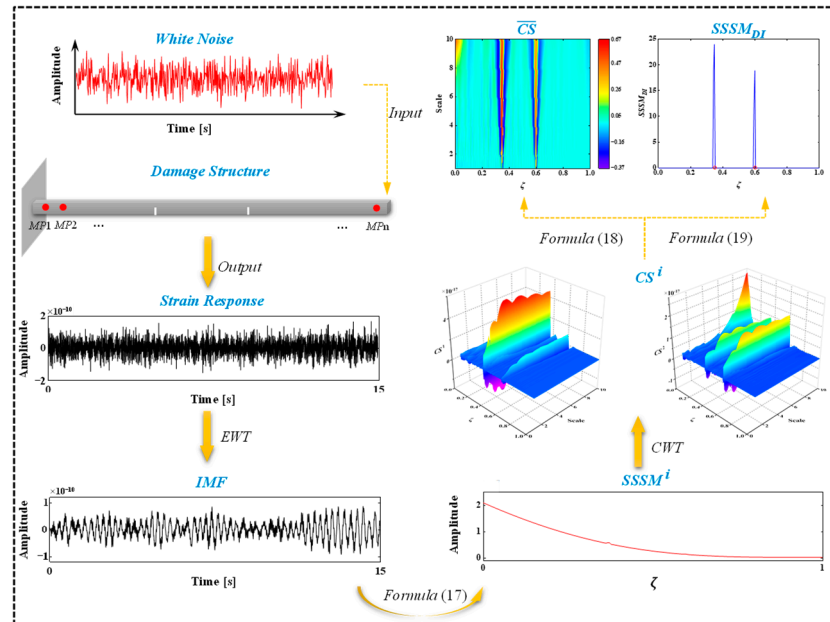


Figure 1. Flow chart of CWT-SSSM feature-based damage identification.

However, it is worth noting that CWT has a boundary problem. Take the CWT mode shape of the free-free (FF) beam as an example. Figure 2a shows the third mode shape of the FF beam, and Figure 3a shows the corresponding third CWT mode shape (choosing the gauss wavelet). It can be seen from Figure 3 that the CWT coefficients at the free end have significant mutations (boundary distortion). If there is damage in the beam, then the extremely high value of the boundary is likely to conceal the abrupt change caused by the damage. To deal with the boundary distortion, iterative weighted least squares fitting

(IWLSF) is introduced to extend the boundary of the third mode shape [33], and the IWLSF theory is detailed in Appendix A. Figure 2b shows the third mode shape after the extension, and Figure 3b shows the third CWT mode shape after the extension. It can be seen from Figure 3 that after extending the boundary, there is no significant abrupt change in the CWT coefficient graph at the free end, and the boundary distortion is significantly reduced.

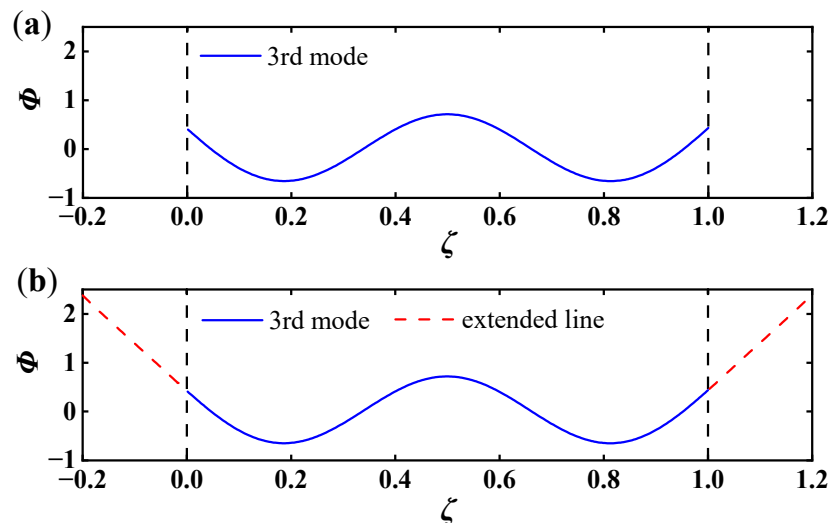


Figure 2. Third mode shape of the FF beam: (a) no boundary extension; (b) boundary extension.

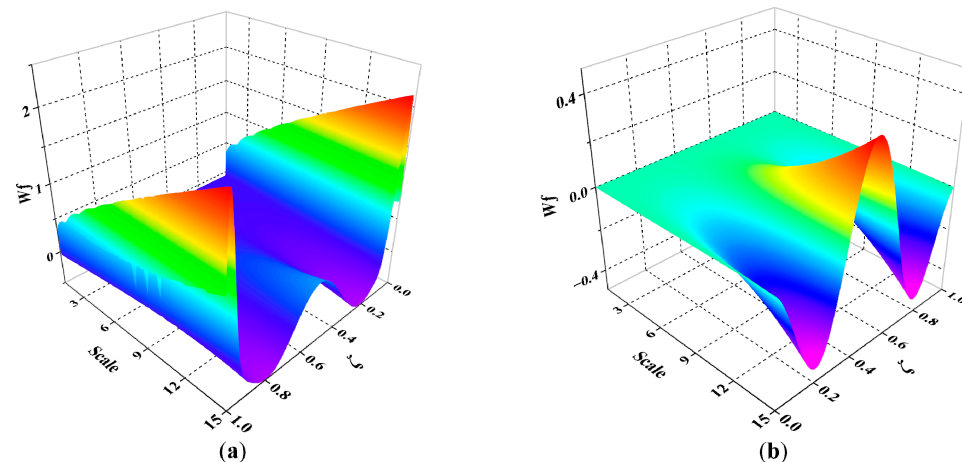


Figure 3. Third CWT mode shape of the FF beam: (a) no boundary extension; (b) boundary extension.

4. Identification of Breathing Cracks in Beams

In this section, a damaged cantilever beam model containing two breathing cracks is established, two damage scenarios with different damage severities are set, and the CWT-SSSM feature-based method is used for crack detection.

4.1. Vibration Model of a Beam Containing Breathing Cracks

Figure 4 shows a typical open cracked beam element with a rectangular cross-section, the element length is L , the width is b , the height is h , the cross-sectional area is A . The modulus of elasticity, Poisson's ratio, and density of the material are E , μ , and ρ , respectively, and the moment of inertia is I . There are two nodes i and j on the element, i is fixed, and there is an open crack of depth a at the distance L_c from the node j . According to the above conditions, the strain energy $W^{(0)}$ of the beam element in the absence of cracks and the additional strain energy $W^{(1)}$ caused by the cracks can be expressed as the following formula [34,35], respectively.

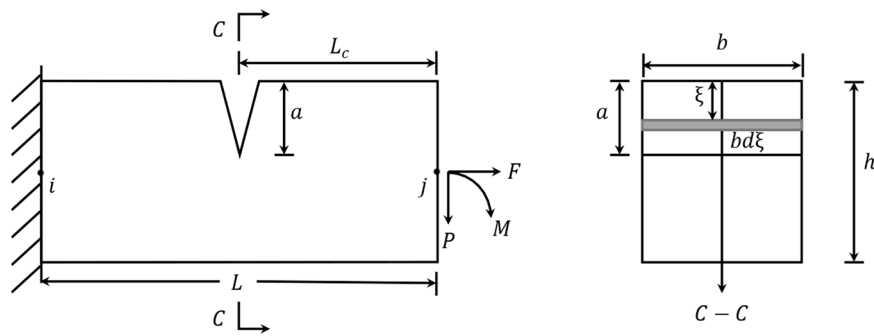


Figure 4. Open cracked beam element.

$$W^{(0)} = \frac{1}{2EI} \left(M^2 L + MPL^2 + \frac{P^2 L^3}{3} \right) + \frac{F^2 L}{2EA} \quad (22)$$

$$W^{(1)} = \int_{A_e} \frac{1}{E'} [(K_{I1} + K_{I2} + K_{I3})^2 + K_{II2}^2] dA \quad (23)$$

where $E' = E$ when it is a plane stress state and $E' = E/(1-\mu^2)$ when it is a plane strain state; A_e is the effective area of the crack. K_{I1} , K_{I2} , K_{I3} , and K_{II2} are the stress intensity factors corresponding to the axial force F , shear force P , and bending moment M . They can be expressed as:

$$K_{I1} = \frac{F}{bh} \sqrt{\pi \xi} F_1 \left(\frac{\xi}{h} \right) \quad (24)$$

$$K_{I2} = \frac{6PL_c}{bh^2} \sqrt{\pi \xi} F_2 \left(\frac{\xi}{h} \right) \quad (25)$$

$$K_{I3} = \frac{6M}{bh^2} \sqrt{\pi \xi} F_2 \left(\frac{\xi}{h} \right) \quad (26)$$

$$K_{II2} = \frac{P}{bh} \sqrt{\pi \xi} F_{II} \left(\frac{\xi}{h} \right) \quad (27)$$

where ξ is the crack depth in the integration process from 0 to the final depth a . F_1 , F_2 , and F_{II} are the modified coefficients of the stress intensity factor, and if $s = \xi/h$, then the modified coefficients can be written as the following formulae:

$$F_1(s) = \sqrt{\frac{\tan(\pi s/2)}{(\pi s/2)}} \frac{0.752 + 2.02s + 0.37(1 - \sin(\pi s/2))^3}{\cos(\pi s/2)} \quad (28)$$

$$F_2(s) = \sqrt{\frac{\tan(\pi s/2)}{(\pi s/2)}} \frac{0.923 + 0.199(1 - \sin(\pi s/2))^4}{\cos(\pi s/2)} \quad (29)$$

$$F_{II}(s) = \frac{1.122 - 0.561s + 0.085s^2 + 0.180s^3}{\sqrt{1-s}} \quad (30)$$

According to Castiglione's theorem, the partial derivative transformation of Formulas (22) and (23) yields the flexibility matrix $c_{ij}^{(0)}$ of the intact beam element and the additional flexibility matrix $c_{ij}^{(1)}$ of the open cracked beam element.

$$c_{ij}^{(0)} = \frac{\partial^2 W^{(0)}}{\partial D_i \partial D_j}; i, j = 1, 2, 3; D_1 = F, D_2 = P, D_3 = M \quad (31)$$

$$c_{ij}^{(1)} = \frac{\partial^2 W^{(1)}}{\partial D_i \partial D_j}; i, j = 1, 2, 3; D_1 = F, D_2 = P, D_3 = M \quad (32)$$

The above analysis is for an open cracked beam element that is fixed at the left end and subjected to forces at the right end. For an open cracked beam element in the FEM coordinate system, in the case of both nodes i and j are subjected to the axial force F , shear force P , and bending moment M and the additional flexibility matrix $c_{ij}^{(\text{add})}$ caused by the crack can be expressed as:

$$c_{ij}^{(\text{add})} = \begin{bmatrix} c_{11}^{(1)} & -c_{12}^{(1)} & -c_{13}^{(1)} \\ -c_{21}^{(1)} & c_{22}^{(1)} & c_{23}^{(1)} \\ -c_{31}^{(1)} & c_{32}^{(1)} & c_{33}^{(1)} \end{bmatrix} \quad (33)$$

The relationship between the forces and displacements in the intact beam element is described by the flexibility matrix $c_{ij}^{(\text{int})}$, where $c_{ij}^{(\text{int})} = c_{ij}^{(0)}$, and the total flexibility matrix $c_{ij}^{(\text{tot})}$ of the open cracked beam element can be expressed as:

$$c_{ij}^{(\text{tot})} = c_{ij}^{(\text{int})} + c_{ij}^{(\text{add})} = \begin{bmatrix} \frac{L}{EA} + c_{11}^{(1)} & -c_{12}^{(1)} & -c_{13}^{(1)} \\ -c_{21}^{(1)} & \frac{L^3}{3EI} + c_{22}^{(1)} & \frac{L^2}{2EI} + c_{23}^{(1)} \\ -c_{31}^{(1)} & \frac{L^2}{2EI} + c_{32}^{(1)} & \frac{L}{EI} + c_{33}^{(1)} \end{bmatrix} \quad (34)$$

On the basis of the above analysis, the stiffness matrix K_{eo} of the open cracked beam element can be written as:

$$K_{eo} = T(c_{ij}^{(\text{tot})})^{-1}T^T \quad (35)$$

where T is the transformation matrix, which can be expressed as:

$$T = \begin{bmatrix} -1 & 0 & 0 & 1 & 0 & 0 \\ 0 & -1 & -L & 0 & 1 & 0 \\ 0 & 0 & -1 & 0 & 0 & 1 \end{bmatrix}^T \quad (36)$$

In fact, cracks under dynamic loading have a ‘breathing effect’. A simple way to construct the stiffness matrix of the breathing cracked beam element is to use the ratio of the instantaneous curvature at the crack to the maximum curvature to determine the degree of opening and closing in the breathing crack [36], which is expressed as the following formula:

$$K_{ec} = K_e + \frac{1}{2}(K_{eo} - K_e) \left[1 + \frac{d''}{d''_{\max}} \right] \quad (37)$$

$$d'' = \frac{\partial^2 y}{\partial x^2} \quad (38)$$

where K_{ec} is the stiffness matrix of the breathing cracked beam element, K_e is the stiffness matrix of the intact beam element, and d'' is the instantaneous curvature at the crack location. From Formula (37), it can be seen that when d'' reaches the maximum instantaneous curvature d''_{\max} , $K_{ec} = K_{eo}$, the crack is completely opened. When d'' equals to $-d''_{\max}$, $K_{ec} = K_e$ and the crack is completely closed. When $-d''_{\max} < d'' < d''_{\max}$, the cracked beam is in the process of gradually opening or closing. It is worth noting that the value of d''_{\max} is calculated in the case of the crack being fully open ($K_{ec} = K_{eo}$). Using the assumption of Rayleigh damping, the displacement response can be solved using the Newmark- β method. The strain response can be obtained by the second-order numerical differentiation of the displacement response as follows:

$$\varepsilon_i = \frac{x_{i-1} - 2x_i + x_{i+1}}{(L)^2} \frac{h}{2} \quad (39)$$

where ε_i and x_i are the strain and vertical displacement of the i th measurement point, respectively.

The cantilever beam model containing two breathing cracks is established according to the above method, and the relevant parameters of the model are shown in Table 1. The cantilever beam is discretized into 200 two-node beam elements with three degrees of freedom (horizontal translation, vertical translation, and rotation) considered at each node. Two breathing cracks with the same depth were established at $L_1 = 4.2$ m ($\zeta = 0.35$) and $L_2 = 7.2$ m ($\zeta = 0.6$) from the fixed end, respectively. In addition, two damage scenarios are set up according to different crack depths a (see Table 1 for details). The placement of 200 measurement points on all nodes except the fixed end and the reason for setting up a large number of dense measurement points is that the greater the number of measurement points, the greater the accuracy of the damage location. In practical engineering applications, the dynamic response of these dense measurement points can be obtained with the help of modern visual measurement techniques (such as digital image correlation [37] and gradient-based optical flow [38]). The cracked cantilever beam model is shown in Figure 5, and the standard Gaussian white noise excitation is applied at the free end, while the time history of the white noise is shown in Figure 6. The sampling time is set to 15 s, the sampling frequency is 200 Hz, and after extracting the displacement response in the y -direction of the cantilever beam, Formula (39) is used to solve the strain response. Figure 7 shows the strain response of measurement points 75 and 120 under the scenario I.

Table 1. Relevant parameters of the cracked cantilever beam.

Dimensional Parameters		Material Parameters
Length: L (m)	12	Poisson's ratio: μ
Height: h (m)	1	Elastic modulus: E (Pa)
Width: b (m)	1	Density: ρ (kg/m ³)
Crack depth: a (m)	0.05 (scenario I), 0.1 (scenario II)	Damping ratio: ξ

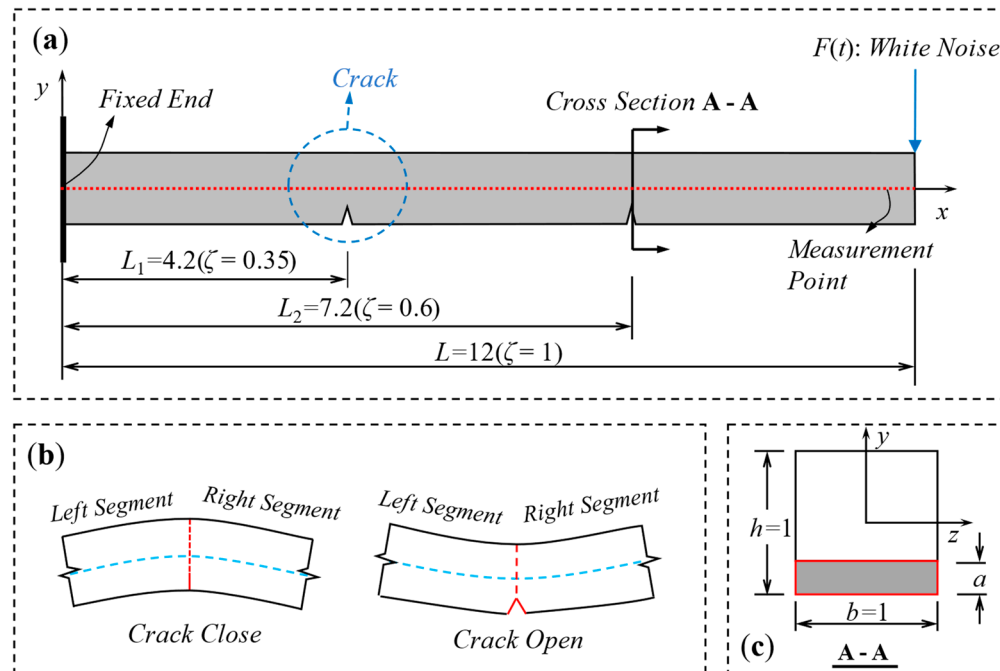


Figure 5. Model diagram of cracked cantilever beam: (a) schematic diagram; (b) crack state; (c) cross section.

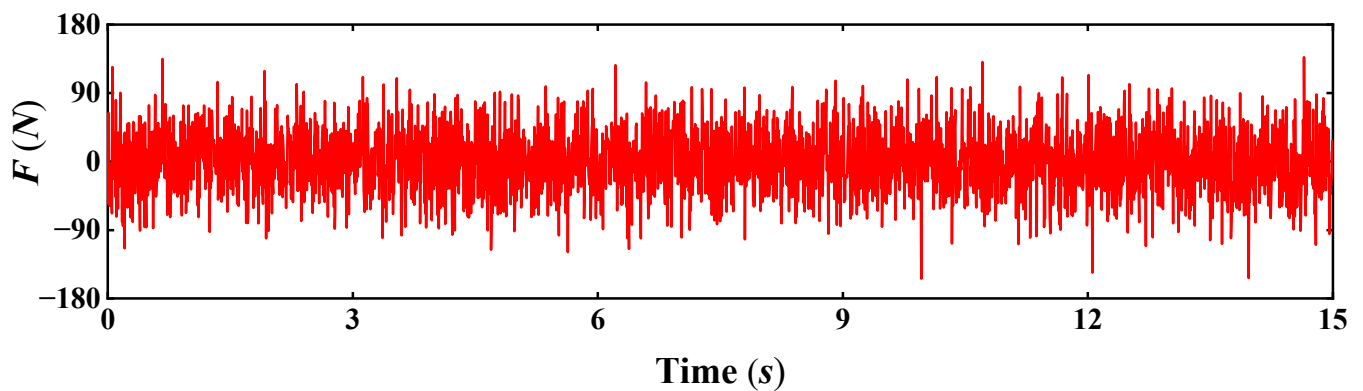


Figure 6. Gaussian white noise time history.

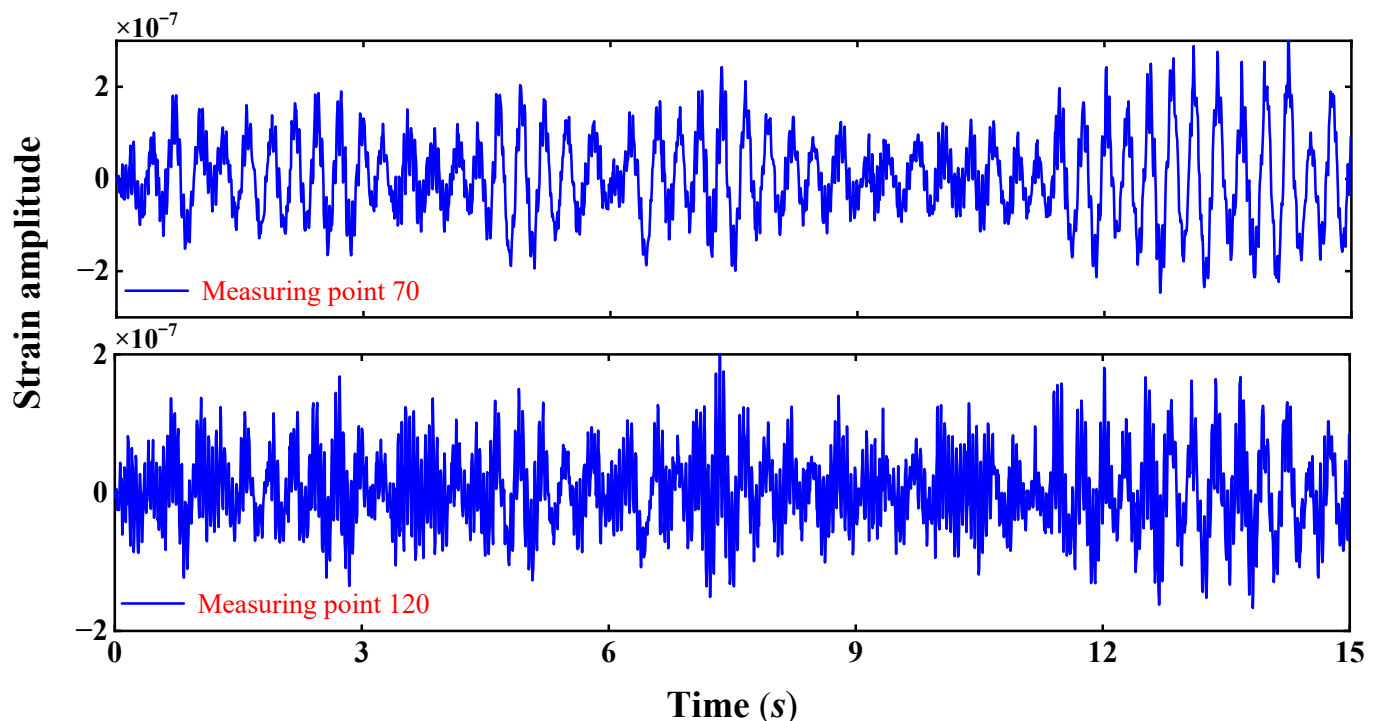


Figure 7. Strain response of cracked cantilever beam under scenario I.

4.2. Calculation of SSSM of Different Orders

To obtain the strain response considering only the i th-order principal vibration, the empirical wavelet transform is applied to the strain response of each measurement point. Taking the strain response of measurement point 120 under scenario I as an example, firstly, the Fourier transform of the response is performed to acquire the spectrum, then the EWT boundary is set to split the spectrum, and finally, the strain component IMF considering only the i th-order principal vibration is separated. Figure 8 shows the spectrum splitting of measurement point 120 under scenario I. Figure 9 shows the first four-strain components after the splitting.

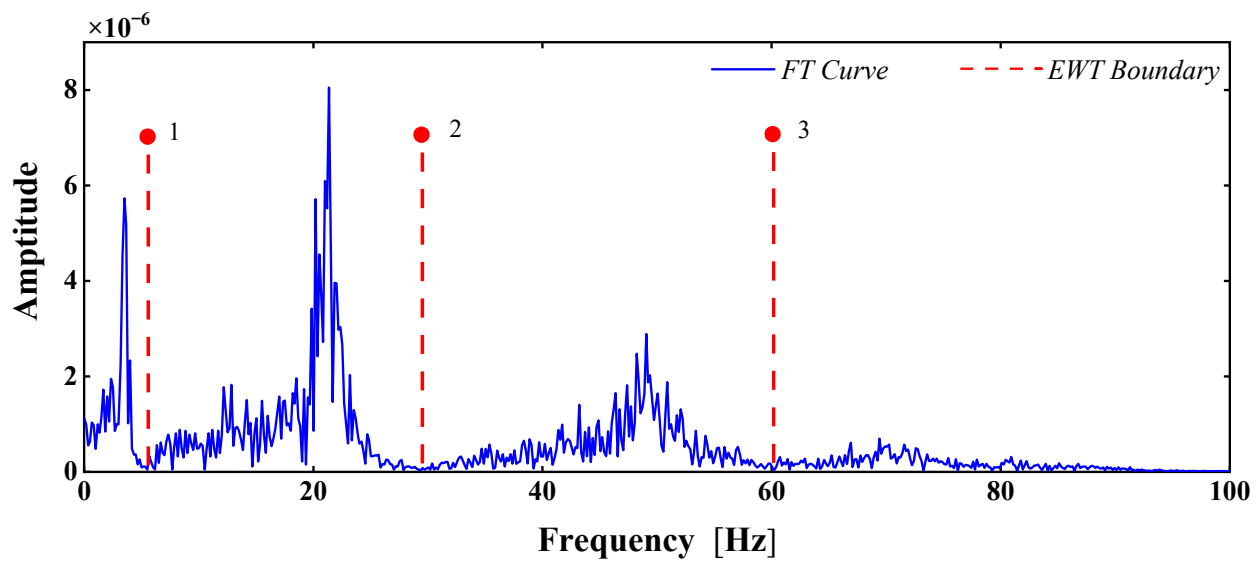


Figure 8. Strain spectrum splitting of measurement point 120 under scenario I.

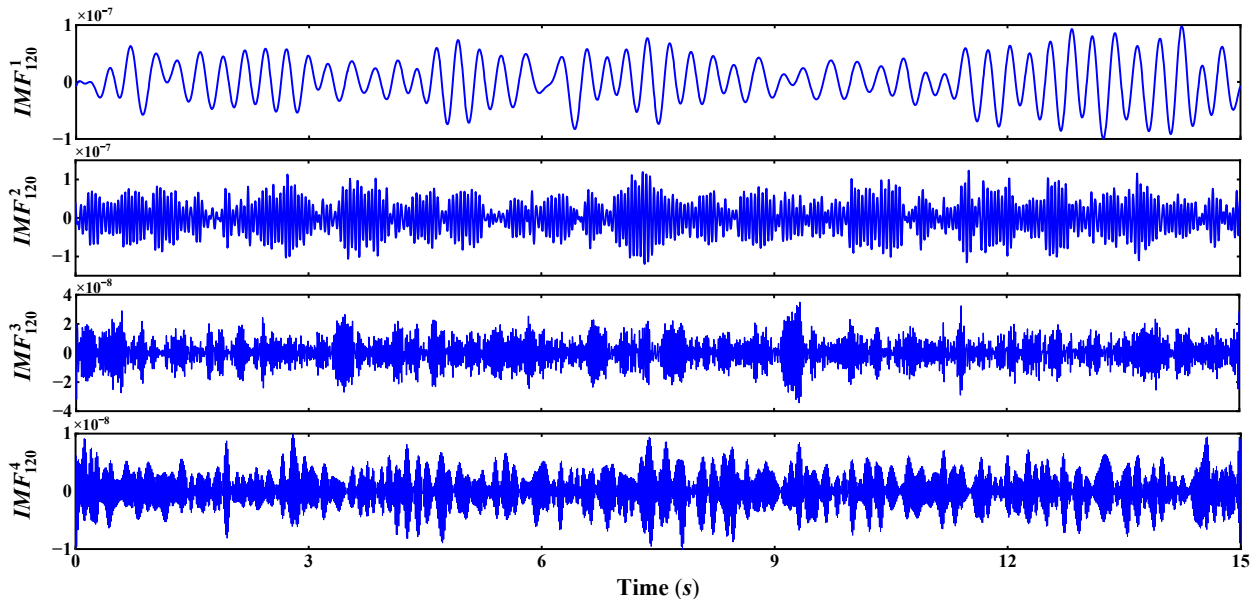


Figure 9. The first four IMF components of measurement point 120 under scenario I.

The IMF_{120}^i acquired by EWT can be substituted directly into Formula (17) to obtain $SSSM_{120}^i$. Repeat the above operation for each measurement point to obtain the $SSSM^i$ of the i th order under scenario I. Figure 10 shows the first four SSSM orders of the cracked cantilever beam in scenario I and II, from which it can be seen that the SSSM curve has a smaller abrupt change at the damage, especially in the multi-damage scenario (scenario I), where the damage severity is small. The direct observation of the SSSM curve is not convenient for judging all the damage locations visually; moreover, it may be misjudged under the influence of uncertainty factors such as noise. To solve this problem, CWT is used to amplify the mutation caused by the damage, and the averaging operation is applied to fuse the damage information in the multi-order SSSM curves, the three-sigma rule is introduced to construct the damage index $SSSM_{DI}$ for the simultaneous identification of multiple damages in the cracked cantilever beams in the following.

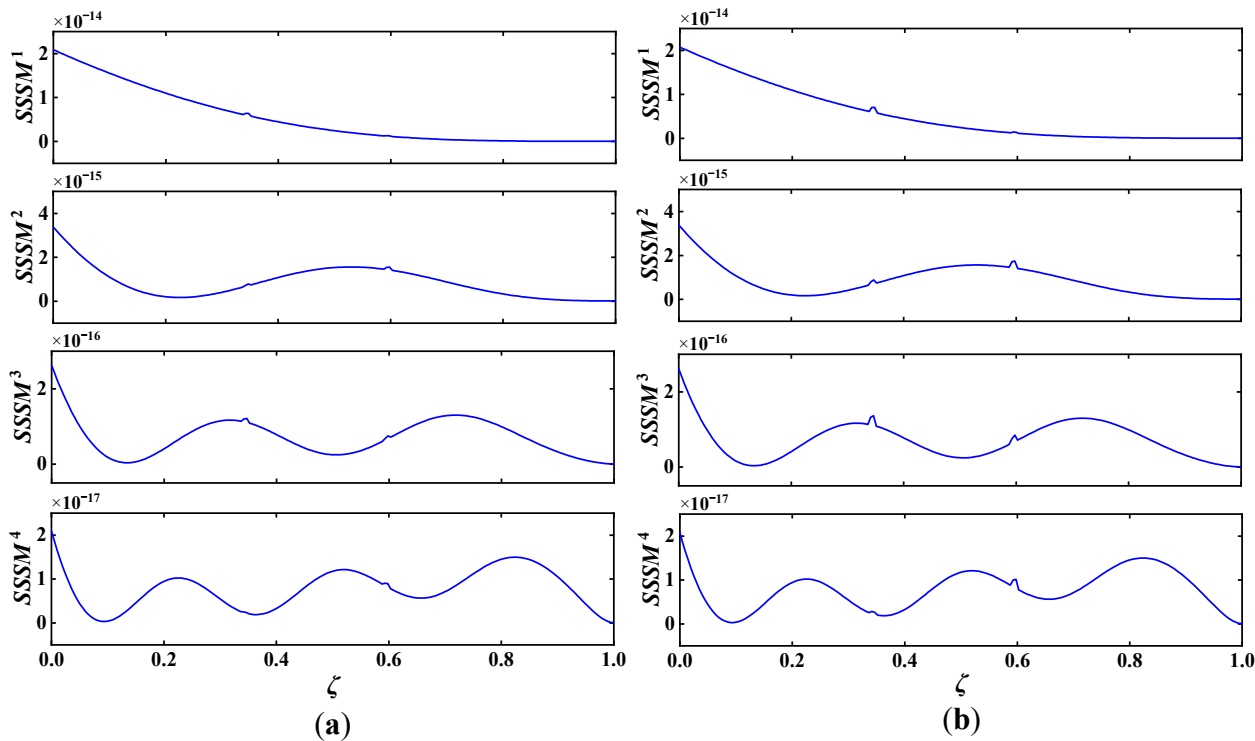


Figure 10. The first four order SSSM of the cracked cantilever beam: (a) scenario I; (b) scenario II.

4.3. Damage Identification Results

The optimal wavelet basis function needs to be determined before CWT. The rbio2.4 wavelet has the following attractive properties [39]: an appropriate number of vanishing moments, compact support, symmetry, biorthogonality, and similarity to the waveform of the signal, which endows the rbio2.4 wavelet with powerful damage feature extraction capabilities. Therefore, in this paper, rbio2.4 is chosen as the optimal wavelet basis function, and the following analysis is based on rbio2.4 wavelets.

Figure 11 shows the first four orders $CS(b, s)$ without the extension boundary under scenario I. From Figure 11, it can be seen that the CWT coefficient of the left boundary is extremely large, and the sudden spikes due to damage are relatively insignificant. In order to reduce the boundary problem, IWLSF is applied to extend the left boundary of each order SSSM curve, and the damage identification is performed using the extended SSSM curve.

Scenario I: a is 0.05 m, and the damage severity is 5%. Scenario II: a is 0.1 m, and the damage severity is 10%. The left boundary of the first four-order SSSM curves under scenarios I and II in Figure 10 is extended. Figures 12 and 14 show the $CS(b, s)$ after extending the boundary under scenarios I and II, respectively. Figures 13 and 15 show the $\bar{CS}(b, s)$ and damage index $SSSM_{DI}$ after fusion under scenarios I and II, respectively, with the actual crack locations ($\zeta = 0.35$ and $\zeta = 0.6$) indicated by the small red circles in the figures. The following conclusions can be drawn from Figures 12–15: ① After the left boundary extension, the boundary distortion is significantly reduced, and there is almost no great abnormal mutation at the boundary. ② The $CS(b, s)$ values of the same order are different at two cracks of the same depth, which means that the sensitivity of $CS(b, s)$ to damage at different locations is different, whereas after fusing the first four order $CS(b, s)$ by averaging, the values of $\bar{CS}(b, s)$ at the two cracks are almost equal. ③ The damage index $SSSM_{DI}$ only mutates at the damage under scenarios I and II, which indicates that the CWT-SSSM feature-based identification method can accurately identify the two crack locations of the cantilever beam and is capable of characterizing slight damage at the same time.

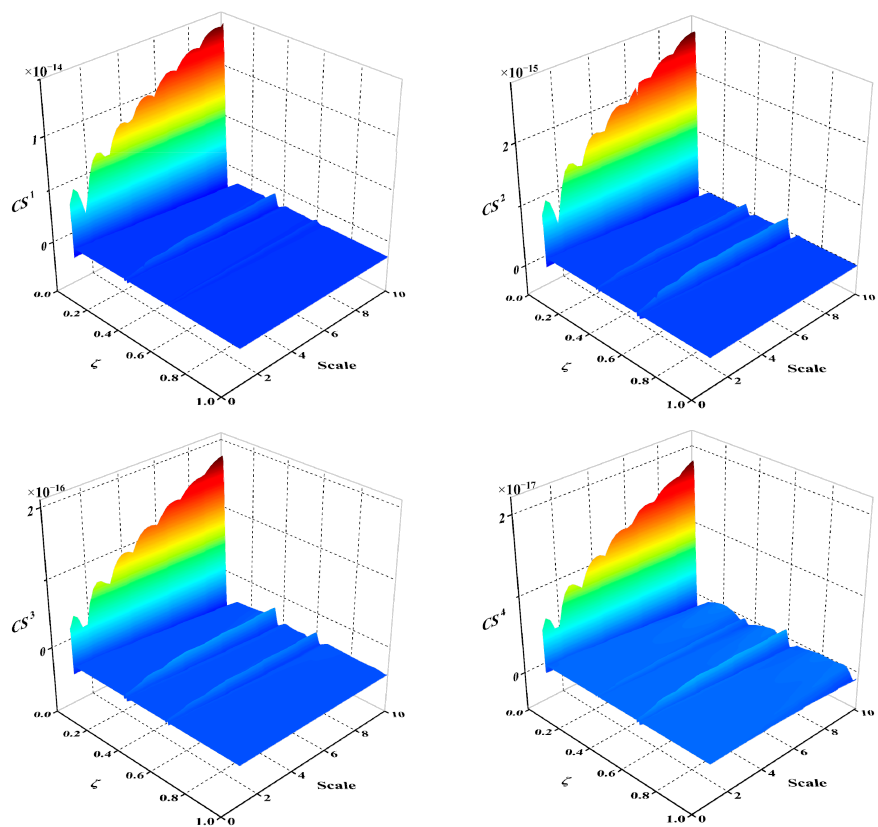


Figure 11. $CS(b, s)$ without extension of SSSM boundary under scenario I.

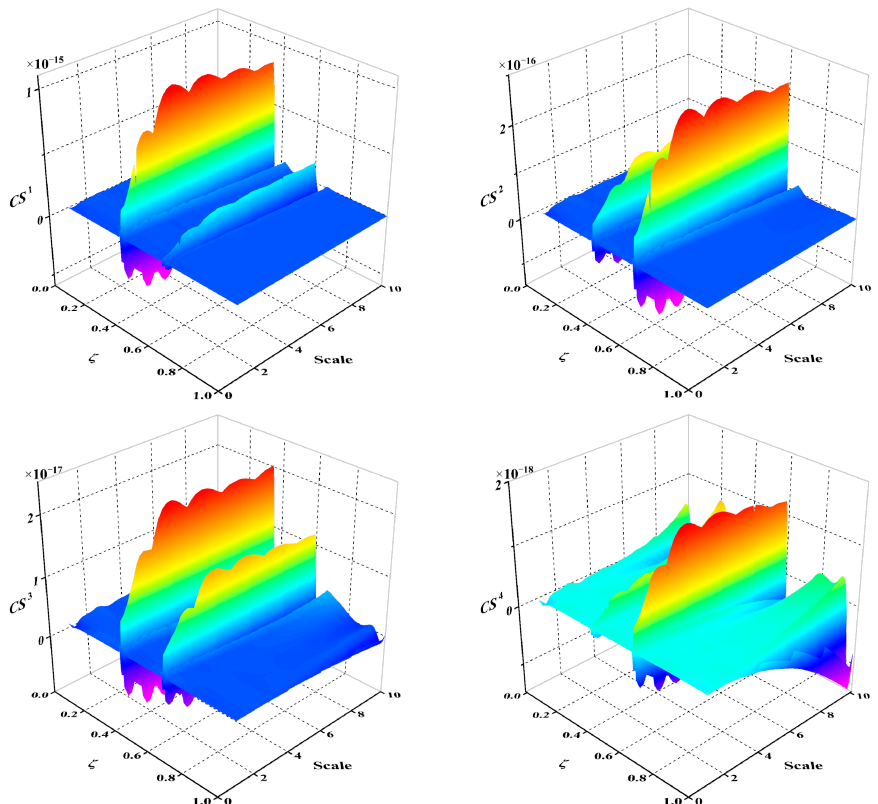


Figure 12. $CS(b, s)$ of the extended SSSM boundary under scenario I.

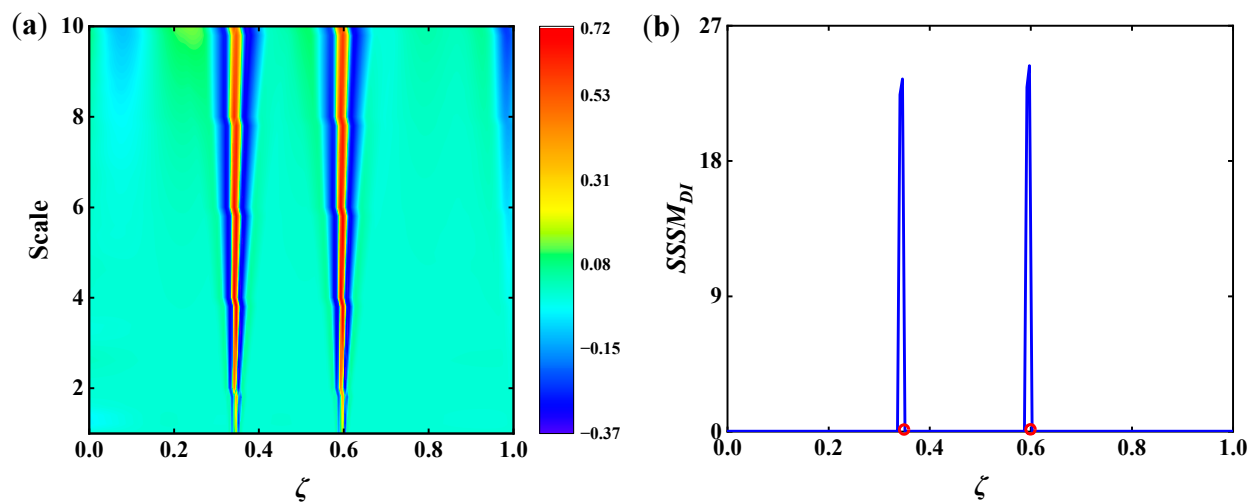


Figure 13. Damage identification results under scenario I: (a) $\bar{CS}(b, s)$; (b) Damage index $SSSM_{DI}$.

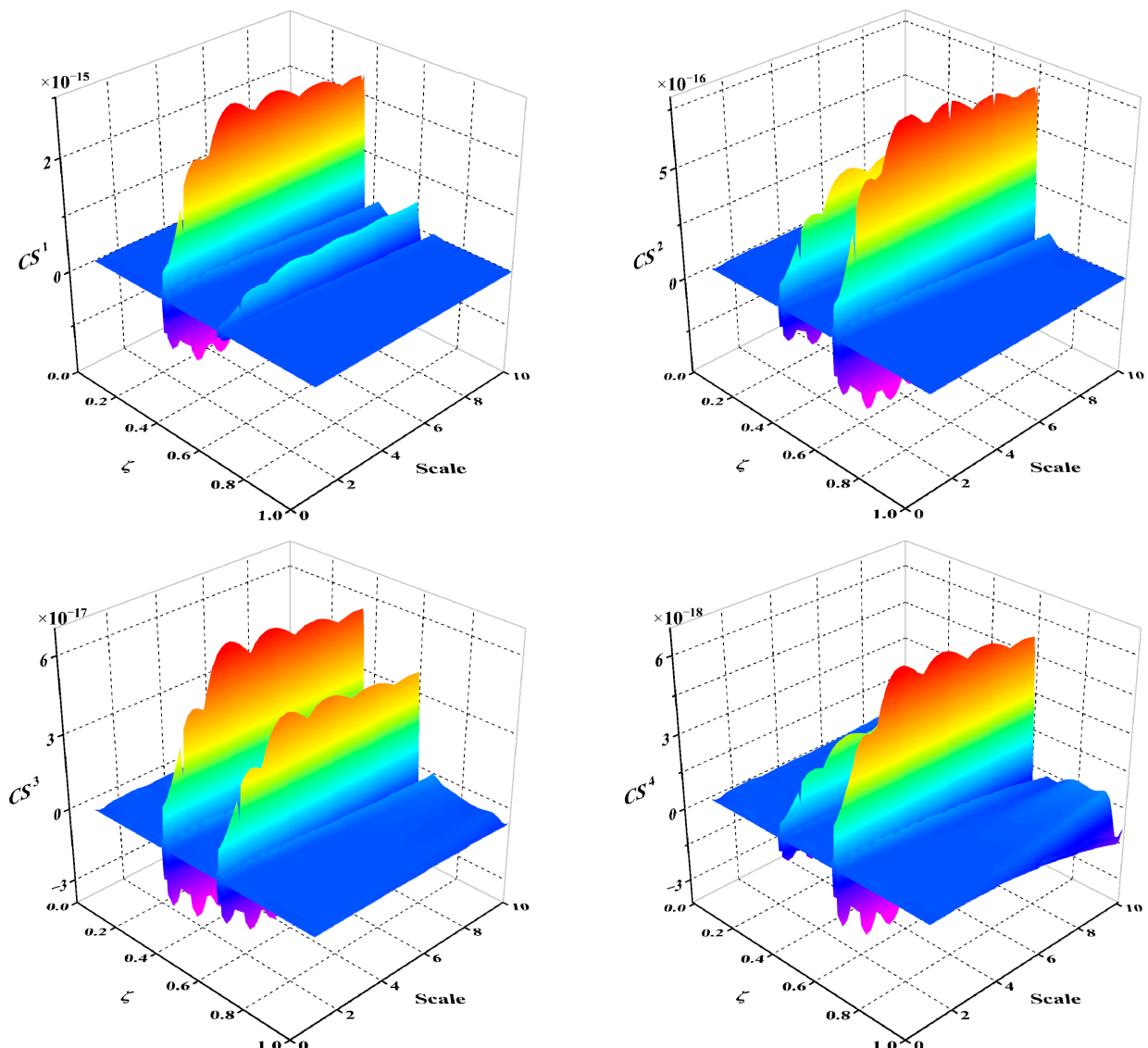


Figure 14. $CS(b, s)$ of the extended SSSM boundary under scenario II.

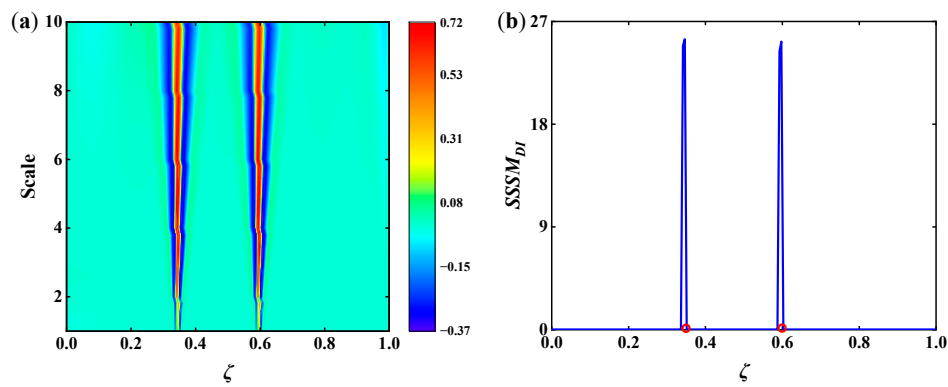


Figure 15. Damage identification results under scenario II: (a) $\overline{CS}(b, s)$; (b) Damage index $SSSM_{DI}$.

5. Noise Robustness and Excitation Adaptability

This section first quantitatively characterizes the noise robustness of the CWT-SSSM feature-based method using a noise immunity index and then discusses the applicability of the proposed method to excitation.

5.1. Robustness Analysis

The measured dynamic response inevitably introduces noise due to environmental noise or equipment limitations. How to accurately detect the damage locations in noisy (or even high noise) conditions is a key issue that must be addressed in the field of structural damage identification [40]. In order to test the noise immunity of the CWT-SSSM feature-based method, the strain response is superimposed with Gaussian white noise, and the response signal containing noise is used for the damage identification study. The noise level γ can be expressed as the following formula:

$$\gamma = \frac{RMS(\varepsilon_{noise})}{RMS(\varepsilon_{signal})} \times 100\% \quad (40)$$

where, $RMS(\varepsilon_{noise})$ and $RMS(\varepsilon_{signal})$ denote the root mean square of white noise and noiseless strain response, respectively, and if the value of γ is larger, it means that the noise intensity is also larger. Take the strain response of measurement point 70 under scenario I as an example, and add the Gaussian white noise of $\gamma = 5\%$, 10% to the strain response, respectively, and the strain response of measurement point 70 after adding the noise is shown in Figure 16.

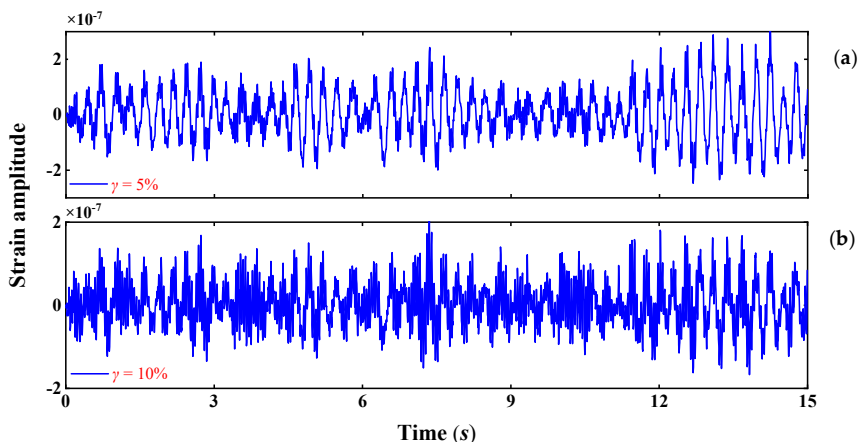


Figure 16. Strain response after adding noise at measurement point 70 under scenario I: (a) $\gamma = 5\%$; (b) $\gamma = 10\%$.

The crack detection of cantilever beams using a strain response containing noise was investigated. Figures 17–20 show the identification results of scenarios I and II under the noise conditions of $\gamma = 5\%$ and $\gamma = 10\%$. It can be seen that $SSSM_{DI}$ accurately indicates the crack location in both $\gamma = 5\%$ and $\gamma = 10\%$ noise conditions, and the value of $SSSM_{DI}$ at the non-destructive location is 0.

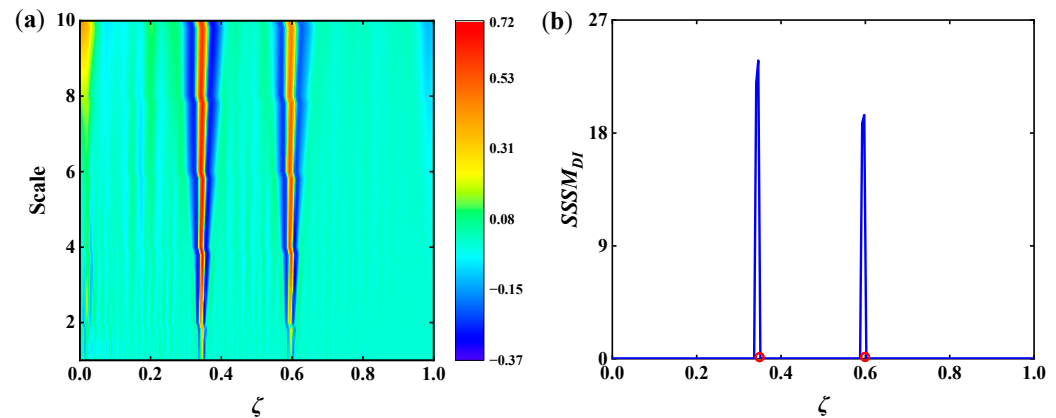


Figure 17. Identification results of cracked cantilever beam under scenario I when $\gamma = 5\%$: (a) $\overline{CS}(b, s)$; (b) Damage index $SSSM_{DI}$.

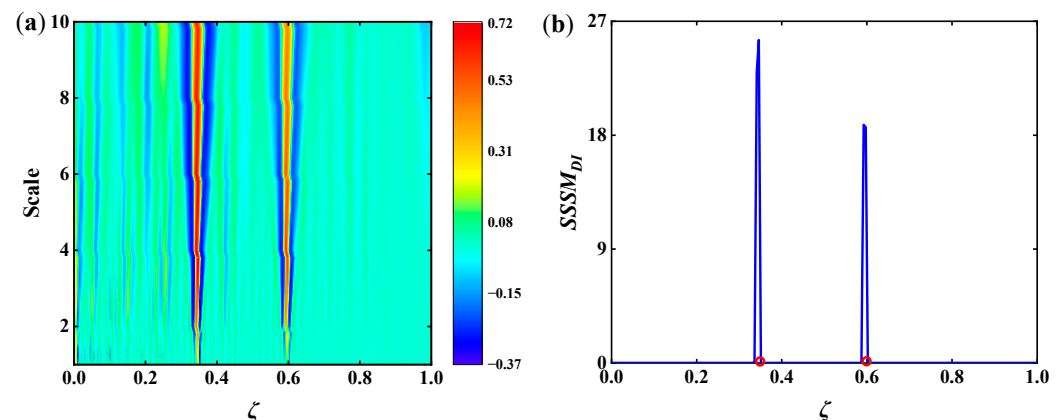


Figure 18. Identification results of cracked cantilever beam under scenario I when $\gamma = 10\%$: (a) $\overline{CS}(b, s)$; (b) Damage index $SSSM_{DI}$.

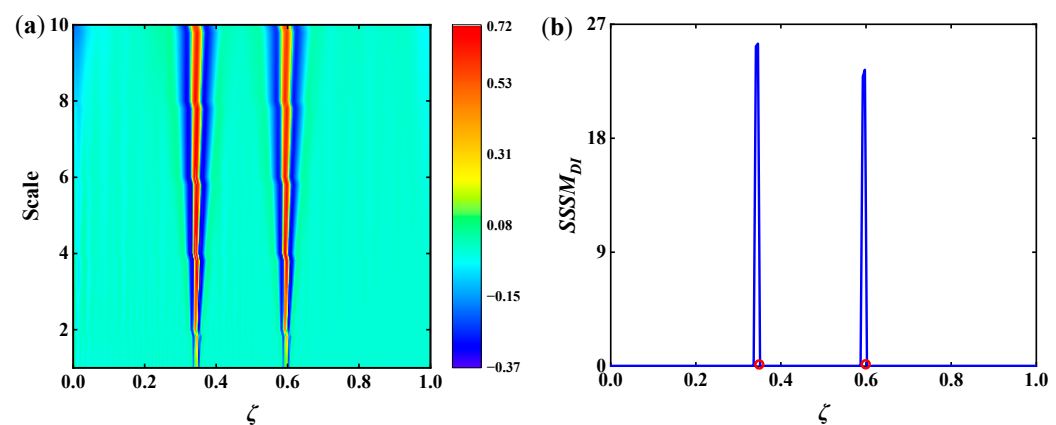


Figure 19. Identification results of cracked cantilever beam under scenario II when $\gamma = 5\%$: (a) $\overline{CS}(b, s)$; (b) Damage index $SSSM_{DI}$.

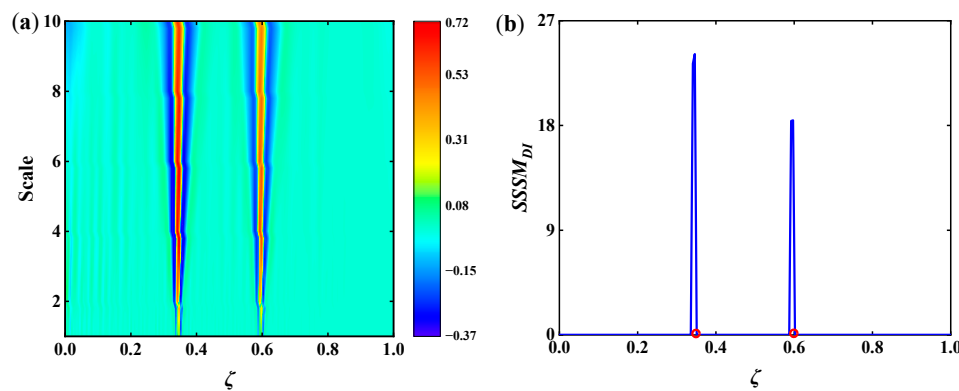


Figure 20. Identification results of cracked cantilever beam under scenario II when $\gamma = 10\%:$ (a) $\overline{CS}(b, s)$; (b) Damage index $SSSM_{DI}$.

Figures 17–20 show the identification results of the once-noise test, which is not representative. In order to quantitatively analyze the noise immunity based on the CWT-SSSM feature method in different noise environments, a noise immunity index (*NII*) is defined according to the Monte Carlo simulation, and the formula of *NII* is shown as follows:

$$NII = (1 - MRR) \times (1 - FRR) \times 100\% \quad (41)$$

where *MRR* is the missing report rate, which represents the probability of missing the actual damage location in *N* tests. *FRR* is the missing report rate, which represents the probability of misreporting the actual damage location in the *N* tests. The essence of *NII* is the probability of identifying the damage without missing and false reports. The larger the *NII*, the higher the accuracy of the proposed method in identifying the actual damage location under noisy conditions, and the better the noise immunity. In this paper, 5000 tests were conducted in $\gamma = \{5\%, 10\%, 15\%, 20\%, 25\%, 30\%, 35\%\}$ noise conditions, and Table 2 shows the results of noise immunity analysis based on the CWT-SSSM feature method in different noise conditions. It can be seen from Table 2 that each *NII* value of $SSSM_{DI}$ is greater than 80% in a $\gamma \leq 20\%$ noise condition under slight damage (scenario I). Each *NII* value of $SSSM_{DI}$ is greater than 90% in a $\gamma \leq 35\%$ noise condition under scenario II. In summary, the CWT-SSSM feature-based baseline-free damage identification method possesses high resistance to noise. Without additional noise reduction algorithms, $SSSM_{DI}$ can identify multiple damage locations of the cracked beams in noisy or even high-noise ($\gamma = 20\%$) conditions.

Table 2. Results of the noise-resistance analysis based on CWT-SSSM feature method in different noise conditions.

Scenario	Index	Noise Level γ						
		5%	10%	15%	20%	25%	30%	35%
I	<i>MRR</i> (%)	0.20	7.20	11.00	15.20	27.80	41.80	61.70
	<i>FRR</i> (%)	0.00	0.00	1.50	5.20	12.10	17.60	26.10
	<i>NII</i> (%)	99.80	92.80	87.67	80.39	63.46	47.96	28.30
II	<i>MRR</i> (%)	0.00	0.00	0.90	1.20	1.20	2.50	8.10
	<i>FRR</i> (%)	0.00	0.00	0.00	0.00	0.00	0.80	1.60
	<i>NII</i> (%)	100.00	100.00	99.10	98.80	98.80	96.72	90.43

5.2. Excitation Adaptability Analysis

The application of the CWT-SSSM feature-based method requires the excitation of Gaussian white noise with a constant power spectral density (uniform spectral excitation). For impulsive loads, its power spectral density is approximately uniform around a finite

number of modal frequencies. A theoretically applied impulsive load can also meet the application requirements of the method in this paper. To verify the applicability of the proposed method to the approximate uniform spectral excitation, an impulsive load of 1000 N is applied to the right end of the breathing cracked cantilever beam. Figure 21 shows the first four order $CS(b, s)$ of scenario I under an impulsive load when $\gamma = 10\%$, Figure 22 shows the $\bar{CS}(b, s)$ and $SSSM_{DI}$ after the averaging operation. The results of the impulsive load are basically consistent with those of white noise, which indicates the applicability of the proposed method for approximate uniform spectral excitation.

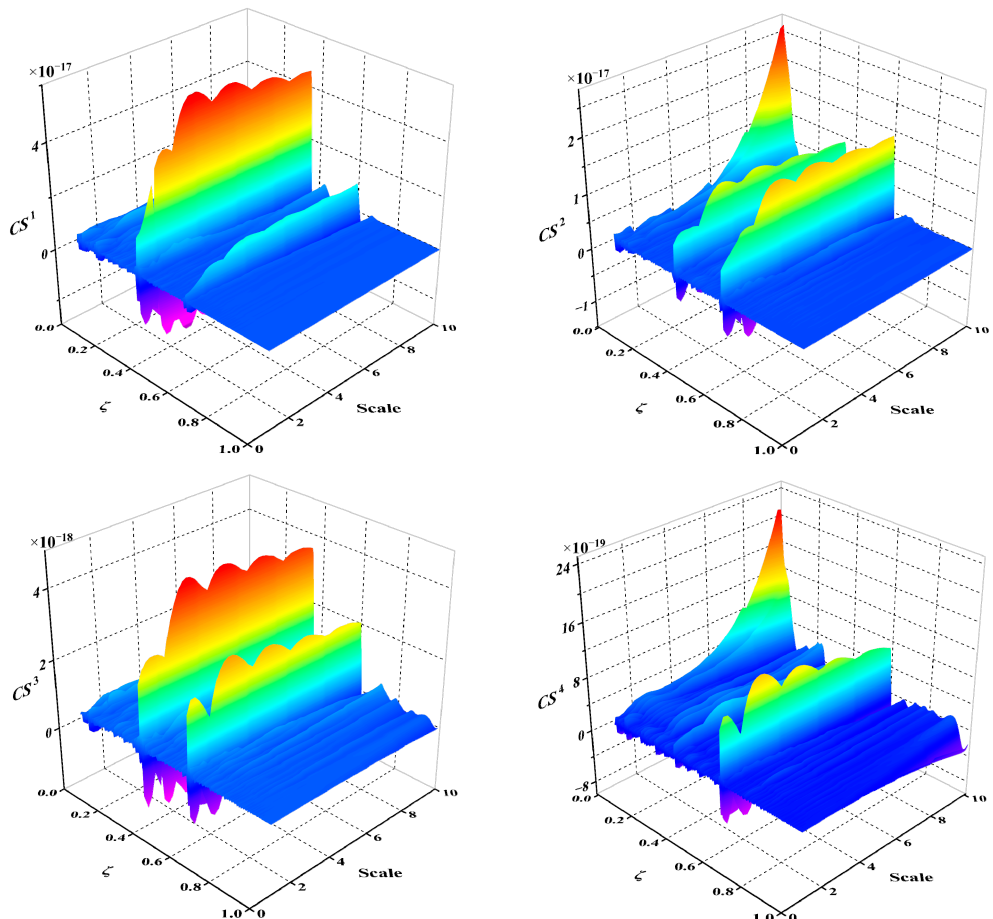


Figure 21. $CS(b, s)$ of scenario I under impulsive load when $\gamma = 10\%$.

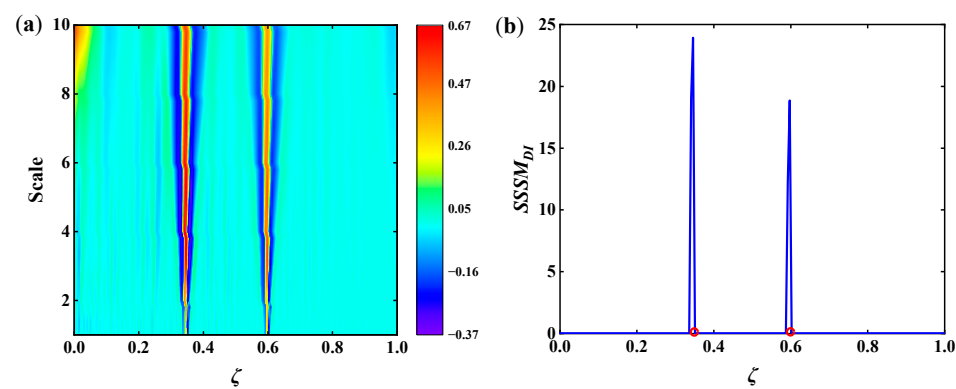


Figure 22. Damage identification results of scenario I under impulsive load when $\gamma = 10\%$:
(a) $\bar{CS}(b, s)$; **(b)** Damage index $SSSM_{DI}$.

6. Conclusions

In this paper, a novel CWT-SSSM feature-based method for the rapid identification of structural damage is proposed. The proposed method uses CWT to amplify the mutations caused by damage, as well as introduce the averaging operation and three-sigma rule to construct a baseline-free damage identification index $SSSM_{DI}$. The proposed method is applied to the numerical simulation studies of a cantilever beam containing two breathing cracks. The numerical results show that $SSSM_{DI}$ is capable of singularity highlighting, damage information fusion, and noise suppression. Under the $\gamma \leq 20\%$ noise condition, $SSSM_{DI}$ can rapidly and accurately detect two slight damages of 5% severity in breathing cracked beams without the need for a complex modal processing procedure and additional noise reduction algorithms, nor does it require known baseline information, geometry, and material parameters of the structure. In addition, the excitation applicability analysis shows that the proposed method is not strictly required for external excitation and is equally suitable for approximate uniform spectral excitation. In future work, it is intended that the dynamic response of dense measurement points will be extracted using visual measurement techniques to further validate the practical applicability of the proposed method.

Author Contributions: Conceptualization, T.D. and M.C.; methodology, T.D. and M.C.; Data curation, J.H. and X.Q.; software, J.H. and M.B.; validation, T.D. and M.C.; writing—original draft preparation, J.H.; writing—original draft preparation, T.D. and M.C.; Visualization, J.H. and X.Q.; funding acquisition, T.D. All authors have read and agreed to the published version of the manuscript.

Funding: The authors are grateful for the support provided by the Key R&D Project of Anhui Science and Technology Department (202004b11020026), the Jiangsu International Joint Research and Development Program (No. BZ2022010), the Nanjing International Joint Research and Development Program (No. 202112003), and the Fundamental Research Funds for the Central Universities (No. B220204002).

Institutional Review Board Statement: Not applicable.

Informed Consent Statement: Not applicable.

Data Availability Statement: Not applicable.

Conflicts of Interest: The authors declare no conflict of interest.

Appendix A

Unlike ordinary least squares fitting (OLSF), iterative weighted least squares fitting (IWLSF) uses a weight function to determine the weight coefficients of each data point; data points with large residuals are given less weight, and the weight coefficients are optimized by iterative iterations. The objective function of IWLSF is:

$$\sum_{i=1}^n w_i (y_i - \varphi(x_i))^2 = \min \quad (\text{A1})$$

where y_i is the measured data, n is the total number of data points, $\varphi(x)$ is the fitted model, and w_i is the weight function. The weight function defined by Huber [35] is used, and its expression is as follows:

$$w_i = \begin{cases} 1, & |u_i| \leq c_h \\ \frac{c_h}{|u_i|}, & |u_i| > c_h \end{cases} \quad (\text{A2})$$

In the above formula, c_h is a constant, which is taken as 1.345, u_i is the residual of the i th data point after normalization, which can be expressed as $u_i = e_i / s$, where e_i is the residual of the i th data point, and s is the residual scale factor, which can be written as the following formula:

$$s = \frac{\text{MAD}(e_1, e_2, \dots, e_i)}{0.6745} \quad (\text{A3})$$

$$\text{MAD}(e_1, e_2, \dots, e_i) = \text{Median}|e_i - \text{Median}(e_1, e_2, \dots, e_i)| \quad (\text{A4})$$

where MAD is the median absolute deviation of the residuals.

For the curve fitting of waveform-type data, the fitted model $\varphi(x)$ uses the trigonometric polynomial:

$$\varphi(x) = a_0 + \sum_{i=1}^n a_i \cos(ix) + b_i \sin(ix) \quad (\text{A5})$$

where a_0 , a_i , and b_i are the coefficients to be estimated and the trigonometric polynomial is very suitable for fitting waveform-type curves. After solving for the coefficients to be estimated using IWLSF, the corresponding amplitudes can be calculated by substituting the horizontal coordinates of the extended region into $\varphi(x)$.

References

- Huang, T.X.; Schroder, K.U. Bayesian probabilistic damage characterization based on a perturbation model using responses at vibration nodes. *Mech. Syst. Signal Process.* **2020**, *139*, 106444. [[CrossRef](#)]
- Aras, F.; Akbas, T.; Eksi, H.; Ceribasi, S. Progressive Damage Analyses of Masonry Buildings by Dynamic Analyses. *Int. J. Civ. Eng.* **2020**, *18*, 903–917. [[CrossRef](#)]
- Mousavi, Z.; Varahram, S.; Ettefagh, M.M.; Sadeghi, M.H.; Razavi, S.N. Deep neural networks-based damage detection using vibration signals of finite element model and real intact state: An evaluation via a lab-scale offshore jacket structure. *Struct. Health Monit.* **2021**, *20*, 379–405. [[CrossRef](#)]
- Ding, Z.H.; Li, J.; Hao, H. Structural damage identification by sparse deep belief network using uncertain and limited data. *Struct. Control Health Monit.* **2020**, *27*, e2522. [[CrossRef](#)]
- Dilena, M.; Morassi, A. Reconstruction Method for Damage Detection in Beams Based on Natural Frequency and Antiresonant Frequency Measurements. *J. Eng. Mech.* **2010**, *136*, 329–344. [[CrossRef](#)]
- Jahangiri, M.; Najafgholipour, M.A.; Dehghan, S.M.; Hadianfar, M.A. The efficiency of a novel identification method for structural damage assessment using the first vibration mode data. *J. Sound Vib.* **2019**, *458*, 1–16. [[CrossRef](#)]
- Fraraccio, G.; Brugger, A.; Betti, R. Identification and damage detection in structures subjected to base excitation. *Exp. Mech.* **2008**, *48*, 521–528. [[CrossRef](#)]
- Ciambella, J.; Pau, A.; Vestroni, F. Modal curvature-based damage localization in weakly damaged continuous beams. *Mech. Syst. Signal Process.* **2019**, *121*, 171–182. [[CrossRef](#)]
- Dewangan, P.; Parey, A.; Hammami, A.; Chaari, F.; Haddar, M. Damage detection in wind turbine gearbox using modal strain energy. *Eng. Fail. Anal.* **2020**, *107*, 104228. [[CrossRef](#)]
- Liu, H.F.; Li, Z.G. An improved generalized flexibility matrix approach for structural damage detection. *Inverse Probl. Sci. Eng.* **2020**, *28*, 877–893. [[CrossRef](#)]
- Li, X.H.; Shi, D.Y.; Yu, Z.H. Nondestructive Damage Testing of Beam Structure Based on Vibration Response Signal Analysis. *Materials* **2020**, *13*, 3301. [[CrossRef](#)] [[PubMed](#)]
- Yanez-Borjas, J.J.; Machorro-Lopez, J.M.; Camarena-Martinez, D.; Valtierra-Rodriguez, M.; Amezquita-Sanchez, J.P.; Carrion-Viramontes, F.J.; Quintana-Rodriguez, J.A. A New Damage Index Based on Statistical Features, PCA, and Mahalanobis Distance for Detecting and Locating Cables Loss in a Cable-Stayed Bridge. *Int. J. Struct. Stab. Dyn.* **2021**, *21*, 1. [[CrossRef](#)]
- Kankanamge, Y.; Hu, Y.F.; Shao, X.Y. Application of wavelet transform in structural health monitoring. *Earthq. Eng. Eng. Vib.* **2020**, *19*, 515–532. [[CrossRef](#)]
- Zhang, J.; Xu, Y.L.; Xia, Y.; Li, J. A new statistical moment-based structural damage detection method. *Struct. Eng. Mech.* **2008**, *30*, 445–466. [[CrossRef](#)]
- Zhang, J.; Xu, Y.L.; Xia, Y.; Li, J. Generalization of the statistical moment-based damage detection method. *Struct. Eng. Mech.* **2011**, *38*, 715–732. [[CrossRef](#)]
- Zhang, J.; Xu, Y.L.; Li, J.; Xia, Y.; Li, J.C. Statistical moment-based structural damage detection method in time domain. *Earthq. Eng. Eng. Vib.* **2013**, *12*, 13–23. [[CrossRef](#)]
- Xiang, W.; Wang, D.S.; Zhu, H.P. Damage Identification in a Plate Structure Based on Strain Statistical Moment. *Adv. Struct. Eng.* **2014**, *17*, 1639–1655. [[CrossRef](#)]
- Wang, D.S.; Xiang, W.; Zhu, H.P. Damage identification in beam type structures based on statistical moment using a two step method. *J. Sound Vib.* **2014**, *333*, 745–760. [[CrossRef](#)]
- Wang, D.S.; Chen, Z.; Xiang, W.; Zhu, H.P. Experimental investigation of damage identification in beam structures based on the strain statistical moment. *Adv. Struct. Eng.* **2017**, *20*, 747–758. [[CrossRef](#)]
- Yang, Z.C.; Yu, Z.F.; Sun, H. On the cross correlation function amplitude vector and its application to structural damage detection. *Mech. Syst. Signal Process.* **2007**, *21*, 2918–2932. [[CrossRef](#)]
- Yoon, M.K.; Heider, D.; Gillespie, J.W., Jr.; Ratcliffe, C.P.; Crane, R.M. Local damage detection using the two-dimensional gapped smoothing method. *J. Sound Vib.* **2005**, *79*, 119–139. [[CrossRef](#)]

22. Wang, N.B.; Ren, W.X.; Huang, T.L. Baseline-free damage detection method for beam structures based on an actual influence line. *Smart Struct. Syst.* **2019**, *24*, 475–490. [[CrossRef](#)]
23. Xu, Y.F.; Kim, J.S. Baseline-Free Structural Damage Identification for Beam-Like Structures Using Curvature Waveforms of Propagating Flexural Waves. *Sensors* **2021**, *21*, 2453. [[CrossRef](#)] [[PubMed](#)]
24. Lu, L.L.; Song, H.W.; Huang, C.G. Experimental investigation of unbound nodes identification for metallic sandwich panels with truss core. *Compos. Struct.* **2017**, *163*, 248–256. [[CrossRef](#)]
25. Rucka, M.; Wilde, K. Application of continuous wavelet transform in vibration based damage detection method for beams and plates. *J. Sound Vib.* **2006**, *297*, 536–550. [[CrossRef](#)]
26. Cao, M.S.; Radzienki, M.; Xu, W.; Ostachowicz, W. Identification of multiple damage in beams based on robust curvature mode shapes. *Mech. Syst. Signal Process.* **2014**, *46*, 468–480. [[CrossRef](#)]
27. Gilles, J. Empirical Wavelet Transform. *IEEE Trans. Signal Process.* **2013**, *61*, 3999–4010. [[CrossRef](#)]
28. Xin, Y.; Hao, H.; Li, J. Operational modal identification of structures based on improved empirical wavelet transform. *Struct. Control Health Monit.* **2019**, *26*, 1545–2255. [[CrossRef](#)]
29. Shi, Q.H.; Hu, K.J.; Wang, L.; Wang, X.J. Uncertain identification method of structural damage for beam-like structures based on strain modes with noises. *Appl. Math. Comput.* **2021**, *390*, 125682. [[CrossRef](#)]
30. Wang, F.D.; Li, R.P.; Xiao, Y.Z.; Deng, Q.T.; Li, X.B.; Song, X.L. A strain modal flexibility method to multiple slight damage localization combined with a data fusion technique. *Measurement* **2021**, *182*, 109647. [[CrossRef](#)]
31. Cui, H.Y.; Peng, W.Q.; Xu, X.; Hong, M. A damage identification method for a thin plate structure based on PVDF sensors and strain mode. *Proc. Inst. Mech. Eng. Part C J. Mech. Eng. Sci.* **2019**, *233*, 4881–4895. [[CrossRef](#)]
32. Gokdag, H. Wavelet-based damage detection method for a beam-type structure carrying moving mass. *Struct. Eng. Mech.* **2011**, *38*, 81–97. [[CrossRef](#)]
33. Lawson, C.; Keats, J.B.; Montgomery, D.C. Comparison of Robust and Least-Squares Regression in Computer-Generated Probability Plots. *IEEE Trans. Reliab.* **1997**, *146*, 108–115. [[CrossRef](#)]
34. Qian, G.L.; Gu, S.N.; Jiang, J.S. The dynamic behaviour and crack detection of a beam with a crack. *J. Sound Vib.* **1990**, *138*, 233–243. [[CrossRef](#)]
35. Zheng, D.Y.; Kessissoglou, N.J. Free vibration analysis of a cracked beam by finite element method. *J. Sound Vib.* **2004**, *273*, 457–475. [[CrossRef](#)]
36. Ariaei, A.; Ziae-Rad, S.; Ghayour, M. Vibration analysis of beams with open and breathing cracks subjected to moving masses. *J. Sound Vib.* **2009**, *326*, 709–724. [[CrossRef](#)]
37. Peters, W.H.; Ranson, W.F. Digital Imaging Techniques in Experimental Stress Analysis. *Opt. Eng.* **1982**, *21*, 213427. [[CrossRef](#)]
38. Javh, J.; Slavic, J.; Boltezar, M. The subpixel resolution of optical-flow-based modal analysis. *Mech. Syst. Signal Process.* **2017**, *88*, 89–99. [[CrossRef](#)]
39. Cao, M.S.; Qiao, P.Z. Integrated wavelet transform and its application to vibration mode shapes for the damage detection of beam-type structures. *Smart Mater. Struct.* **2008**, *17*, 055014. [[CrossRef](#)]
40. Deng, T.F.; Huang, J.W.; Cao, M.S.; Li, D.Y.; Bayat, M. Seismic Damage Identification Method for Curved Beam Bridges Based on Wavelet Packet Norm Entropy. *Sensors* **2022**, *22*, 239. [[CrossRef](#)]